Submitted to Nuclear Physics B

PUB-76-141-E FERMILAB-PUB-76-141-E #154

CROSS SECTIONS AND CHARGED MULTIPLICITY DISTRIBUTIONS FOR $\pi^- p$ and $K^- p$ INTERACTIONS AT 147 GeV/c.*

D. Fong, M. Heller, A. M. Shapiro, M. Widgoff
Brown University, Providence, Rhode Island 02912

F. Bruyant
CERN, Geneva 23, Switzerland

D. Bogert, M. Johnson
Fermilab, Batavia, Illinois 60510

R. Burnstein, C. Fu, D. Petersen, M. Robertson, H. Rubin
Illinois Institute of Technology, Chicago, Illinois 60616

R. Sard, A. Snyder, J. Tortora
University of Illinois, Urbana, Illinois 61801

D. Alyea
Indiana University, Bloomington, Indiana 47401

C-Y Chien, P. Lucas, A. Pevsner, R. Zdanis
Johns Hopkins University, Baltimore, Maryland 21218

J. Brau*1, J. Grunhaus*2, E. S. Hafen, R. I. Hulsizer, U. Karshon*3,
V. Kistiakowsky, A. Levy*4, A. Napier, I. A. Pless, J. Silverman,
P. C. Trepagnier, J. Wolfson, R. K. Yamamoto
Massachusetts Institute of Technology, Cambridge, Massachusetts 02139

H. Cohn
Oak Ridge National Laboratory, Oak Ridge, Tennessee 37830

T. C. Ou, R. Plano, T. Watts
Rutgers University, New Brunswick, New Jersey 08903

E. Brucker, E. Koller, P. Stamer, S. Taylor
Stevens Institute of Technology, Hoboken, New Jersey 07030

W. Bugg, G. Condo, T. Handler, E. Hart
University of Tennessee, Knoxville, Tennessee 37916

H. Kraybill, D. Ljung, T. Ludlam, H. D. Taft
Yale University, New Haven, Connecticut 06520

*This work supported in part by the U.S. Energy Research and Development Administration and the National Science Foundation

*1 Fannie and John Hertz Foundation Fellow

*2 On leave of absence, Tel-Aviv University, Israel

*3 On leave of absence, the Weizmann Institute of Science, Israel

*4 Present Address, Tel-Aviv University, Israel

ABSTRACT

The results presented in this paper were obtained from a 105,000-frame exposure of the FNAL Hybrid Proportional Wire Chamber-30-inch Bubble Chamber System, in a tagged beam of 147 GeV/c negative particles. Elastic, total and topological cross sections were obtained for both $\pi^- p$ and $K^- p$ interactions. Comparisons with other data, taken with various beam particles over large momentum intervals, show good agreement with KNO scaling, and similarity in the scaling behavior of σ_n for the different beam particles.

I. INTRODUCTION

This paper presents the total, elastic and topological cross sections for $\pi^- p$ interactions at 147 GeV/c, together with similar information for K^- mesons of the same momentum, the π-K separation being accomplished by means of a Čerenkov signal. These results are based on approximately 15,000 events from the complete analysis of a 105,000 - frame exposure of the Fermilab Hybrid Proportional Wire Chamber - 30-inch Bubble Chamber System in a tagged beam of negative particles of 147 GeV/c momentum. An analysis of a portion of the data was presented in a previous paper.[1]

The hybrid system, developed by the PHS Consortium, is briefly described. The cross section results and multiplicity distributions are given and are compared with results obtained in other experiments at various momenta and with different beam particles.

II. EXPERIMENTAL PROCEDURE

A. Apparatus

Fig. 1 is a schematic representation of the hybrid system with the 30-inch bubble chamber as target, and with spectrometer elements both upstream and downstream. The spectrometer is composed of multi-wire proportional chambers (PWC's) at locations A-G, and makes use of the bubble chamber magnetic field. The upstream portion, the beam-tagging telescope, utilizes PWC's with 2 mm wire spacing and 10 cm x 10 cm active area whereas the downstream multiparticle spectrometer portion utilizes PWC's with 2 mm wire spacing and 31 cm x 31 cm active area. The counter at each of the detector locations A-G is made up basically of three planes of wires, the wire direction in a given plane being oriented at 120 degrees with

respect to the other planes of the triplet. Counters D, F and G include additional staggered wire planes for greater measurement precision. The upstream system also includes a Čerenkov counter;[2] the downstream system includes a muon counter, and a γ detector consisting of a PWC triplet at location H, behind 0.5 inch of lead. The muon detector, situated downstream of the entire spectrometer, consists of 100 cm of lead followed by a 30 cm x 60 cm x 0.6 cm scintillator which in turn is backed up by 320 cm of concrete and another scintillator.

The signal pulse from each sense wire in the system is discriminated and amplified in the immediate locality of the planes. All signals are brought into an area near B and a master gate, formed by a coincidence from scintillators SC_1 and SC_2, is used to strobe all signals into local memory. The signals from the Čerenkov counter and the μ detector are treated as if they originated from proportional chamber sense wires and are also strobed into local memory. The transmission cables provide the time delay necessary to form the master strobe gate. During this experiment the width of the gate was set at $\sim$75 nsecs and an additional 50 nsecs of dead time was imposed by the storage system to allow the individual particle signals to be recorded unambiguously. Every sense wire in the system and each of the pseudo-wires used for tag signals has its own 16-bit local memory word which allows storage of time-correlated information for 16 incident beam particles at a rate of $\sim$8 MHz. Particle identification is thus accomplished for each particle individually. At the end of a bubble chamber spill, the local memory is read out into a computer. The scanning of the local memory is done by hardware at a rate of 250 KHz.

The trajectory of each particle through both upstream and downstream

sections of the spectrometer is determined by least-squares fit of the straight line particle path, outside any magnetic field region, to coordinates determined from the individually known PWC wires that have recorded hits. The trajectory is then extrapolated through the magnetic field region to the track in the bubble chamber in order to obtain the particle momentum. These procedures are carried out wholly by off-line computer programs.[3,4]

B. Beam

During this experiment, the beam was set to deliver to the hybrid system negative pions of 147 GeV/c momentum, with a measured dispersion $\Delta p/p \sim 0.9$ percent. The spatial definition of each particle trajectory was accomplished by the upstream telescope portion of the PWC spectrometer as described in Section IIA.

Identification of each particle in the beam was obtained from the Čerenkov counter and the muon detector. The composition of the beam in the bubble chamber, with corrections made for interactions in the upstream wall, was found to be: π^-, 94.2 ± 0.1 percent; K^-, 1.9 ± 0.1 percent; $\bar{p}$, 1.3 ± 0.1 percent; and μ^-, 2.6 ± 0.1 percent. The quoted errors are statistical.

C. Scanning and Event Reconstruction

For the π^- data, the bubble chamber film was scanned for all events in a fiducial volume defined to give sufficient track length of the primary to check its direction, and sufficient downstream length to allow fast forward-going tracks to separate. Approximately 16 percent of the 16,460 events found were not measured by the scanners, 10.4 percent because the frames were overcrowded, having more than 10 beam tracks or

background tracks entering the fiducial volume, and 5.3 percent because the events were judged unmeasurable, usually because a secondary interaction occurred very close to the primary. The remaining events were predigitized as they were found, then measured by the automatic system PEPR. View-to-view track matching was done in the geometry reconstruction program GEOMAT.[5] The location of the primary interaction vertex reconstructed by this program was then compared with the expected trajectories of the beam particles entering the chamber, as determined by their signals in the upstream PWC's,[4] in order to establish the identity of the interacting particle, and to identify the accompanying signals of the forward-going secondaries in the downstream PWC system.

The trajectories of particles in the downstream PWC's were reconstructed by means of the program PWGP,[4] using the coordinates determined by the wires activated by the particle. These trajectories were then extrapolated back to the chamber, and matched to track measurements in the bubble chamber. The linking of track trajectories in the bubble chamber and the downstream system was carried out by means of the program TRACK ORGANIZER.[6]

D. Effective Track Length

For the $\pi^- p$ cross section calculations, all the events as found by the scanners were counted, except those in the overcrowded frames. Beam counts were made in every ten frames, again excluding overcrowded frames, and the beam composition was determined as described in Section IIB. Correction was made for the μ^- contamination of 2.6 percent. The correction for K^- and $\bar{p}$ in the beam amounted to a 0.6 percent effect on the total cross section, as determined from the percentages of K^- and $\bar{p}$ in

the beam and the total cross sections for K^-p and $\bar{p}p$ interactions given in Reference 7. This 0.6 percent correction was applied to each of the topological cross sections. The fiducial volume used was 44.7 cm along the beam direction, except that in about 24 percent of the film a shorter volume, 26.3 cm, was defined for events with more than two prongs. The density of liquid hydrogen was taken as 0.0627 ± 0.0005 gm/cm^3. The total track length scanned corresponds to $\sigma_{n=2} = (1.392 \pm 0.011)N_2$ μb and $\sigma_{n>2} = (1.552 \pm 0.013)N_n$ μb, where n is the charged particle multiplicity and N_n the true number of events of topology n, obtained from the scanning results as described below.

E. Scanning Corrections

A number of corrections were made to find the numbers N_n of events of charged particle multiplicities n from the numbers found in scanning:

(i) Scanning Efficiencies

The data in this experiment are based on a single scan, and the scanning efficiencies for randomly missed events have been determined by double scanning about 40 percent of the film. These scanning efficiencies, for the various topologies, were found to be: two-prong, 89.6 ± 1.3 percent; four-prong, 95.1 ± 1.1 percent; six-prong, 96.0 ± 0.8 percent; greater than six-prong, 96.2 ± 0.8 percent.

(ii) Low Momentum Transfer

Two-prong events of momentum transfer to the target proton of less than a certain minimum ($|t|<0.04$ (GeV/c)^2) are systematically missed and are not corrected for by double scanning. To estimate the numbers missed, the measured two-prong sample was divided into

elastic and inelastic components and treated as described in Section IIIA. To correct for events missed in the region $0.0 \leq |t| < 0.04$ $(GeV/c)^2$, 16.7 ± 2.8 percent has been added to the elastic sample and 5.2 ± 3.0 percent to the inelastic sample.

(iii) Close Scatters and Short Stubs

Among the 14,750 events included in the sample, 160 had odd numbers of prongs. Such events appeared if a secondary interaction occurred too close to the primary vertex to be distinguished, so that its outgoing tracks were added into the primary prong count, while the connecting track was missed. An odd number of prongs would also result if an outgoing proton had very short range, so that its track was not visible. In order to estimate how large these effects are, the numbers and the distribution in distance from the primary vertex of the observed secondary interactions and of stopping tracks were found as functions of primary topology. For primary interactions with two prongs the efficiency for distinguishing secondary interactions was low for vertex separations of less than 5 mm, and this region of reduced resolution increased to about 20 mm for primary interactions of more than eight prongs. Similar regions of reduced efficiency for perceiving short tracks were determined also. The two effects together are of the correct magnitude to account for the odd-prong topologies observed, the missed short stubs being more important in two-, four- and six-prong events and the close interactions more important at higher multiplicities.

The distribution in prong number of about 1100 observed secondary interactions was determined as a function of primary topology,

and the odd-prong events were distributed statistically into appropriate even topologies in accordance with the relative number of missed short stubs and secondary interactions, and with the prong number distributions of the secondary interactions. The average secondary interaction multiplicity was found to vary slowly, from about 3.3 charged prongs for a primary prong count of 2 or 4, to 2.2 for 16 prong primary interactions, the overall average secondary interaction multiplicity being 2.9 charged prongs.

(iv) Close V^o's and Electron Pairs

Distributions in neutral connecting-track length as a function of topology showed regions close to the primary vertex where secondary V^o and e^+e^- vertices were systematically not resolved, similar to the regions of confusion described in Section IIE(iii). Corrections were made for each topology, on the basis of estimates of the numbers missed, by shifting events to the next lower even topology. Approximately 5 percent of all these secondary vertices are systematically missed, and fewer than one percent of all the events are affected.

(v) Unidentified Dalitz Electrons

The number of Dalitz pairs expected at each topology was calculated by using the preliminary result of this experiment for the mean number of π^o mesons, $[\langle n_\pi \rangle]_n$ per event for each primary charged multiplicity n.[8] The directly determined numbers were used for $n<12$, and a linear extrapolation of the data was used for $n \geq 12$. The value 0.0117 ± 0.0005 was used for the branching ratio for Dalitz production.[9] Dalitz pairs were expected in 550 of the events scanned;

42 percent satisfied the scanning criterion of at least one slow electron and were thus identified. Corrections for the remaining undetected Dalitz pairs at each multiplicity were made by shifting events from an even number topology to the next lower even number, to avoid counting electrons as prongs.

The observed and corrected numbers of events of the various topologies are given in Table I, together with the cross sections.

III. $\pi^- p$ CROSS SECTIONS

A. Two-Prong Interactions, Elastic and Inelastic

The separation of elastic from inelastic two-prong events is essential to the determination of the cross sections and to the analysis of the inelastic interactions. The downstream PWC information provides a sensitive technique for making this separation. As described in References 1 and 10, an accurate identification of elastic events was obtained by using the measured momentum (or range) of the slow recoil proton in the bubble chamber to predict the trajectory of the outgoing pion as it traversed the downstream proportional wire planes. The predicted and observed trajectories were then compared, with a spatial resolution of 0.5 mm and an angular resolution of 0.1 mr in the downstream counters. As a second technique, all 2-prong events were fitted to the four-constraint elastic hypothesis using the kinematic program SQUAW. The results of the two procedures were found to be in excellent agreement. Approximately 5 percent of the two-prong events have no information on the fast outgoing negative track in the downstream PWC's, because this track has scattered either in the liquid hydrogen or the exit window of the bubble chamber. For these

events the results of the SQUAW fit to the bubble chamber measurements were accepted in making the elastic/inelastic assignment. Among the two-prong events found, 62.1 ± 2.1 percent are identified as elastic and 37.9 ± 2.2 percent as inelastic.

The elastic $|t|$ distribution is shown in Fig. 2; it is fitted very well, over the range $0.04 \leq |t| < 0.6$ $(\mathrm{GeV}/c)^2$, by the equation

$$\frac{d\sigma}{dt} = A\, e^{-B|t|}, \qquad (1)$$

where $A = d\sigma/dt|_{t=0} = 26.9 \pm 2.2$ mb/$(\mathrm{GeV}/c)^2$ and $B = 8.29 \pm 0.32$ $(\mathrm{GeV}/c)^{-2}$. The χ^2-value of the fit is 26.8 for 26 degrees of freedom, corresponding to a confidence level of 0.42. The intercept A is within 1.25 standard deviations of the optical point, 29.6 ± 0.2 mb/$(\mathrm{GeV}/c)^2$, derived from the total cross section measurements of Carroll et al.[7]

The elastic channel and the inelastic one with identified protons appear to have systematic losses when there is very low momentum transfer to the target proton. The number of elastic events found with $|t| < 0.04$ $(\mathrm{GeV}/c)^2$, amounts to 49 percent of the number expected in this region, based on extrapolation of the fitted exponential. The number of elastic events has been increased by 16.7 ± 2.8 percent in order to correct for this loss.

The inelastic events with identified proton have a similar $|t|$ distribution[10] and the same percentage loss at low $|t|$ has been assumed for them, while the remaining inelastic events appear to have no comparable loss. The overall result is a low t correction of 5.2 ± 3.0 percent for the entire inelastic sample.

After all corrections have been applied, we determine the total

2-prong cross section to be 5.04 ± 0.15 mb, with 3.24 ± 0.14 mb elastic scattering and 1.80 ± 0.12 mb inelastic scattering.

B. Total Cross Sections

The total $\pi^- p$ cross section measured in this experiment is 24.24 ± 0.29 mb, while the total inelastic cross section is 21.00 ± 0.28 mb. This confirms our preliminary result,[1] and is in excellent agreement with the value $\sigma_{tot}(\pi^- p) = 24.07 \pm 0.06$ mb from reference 7.

C. Topological Cross Sections

The corrections described in Section IIE have been made to the data to obtain the cross sections σ_n for the various topologies. The data and the cross sections are presented in Table I and in Fig. 3. Column 2 of this table lists the observed numbers of events for each topology. Because in part of the experiment different fiducial volumes were used for scanning two-prong events and events of higher multiplicity, the numbers of events in Column 2 are not in proportion. Numbers of events, normalized to the scanning length for n>2 and with all the corrections described in Section IIE carried out, are given in Column 3. In Column 4 the cross sections are given. These cross sections - total, elastic, and topological - have been determined absolutely in the experiment; they have not been normalized to any other measurement.

The values of the inelastic cross sections are plotted with other data[11-14] in Fig. 4, to show the variation of the topological cross sections with momentum of the incoming π^-. Over the momentum region shown in Fig. 4, the 2-prong cross section is seen to be decreasing, at first relatively rapidly, then, above about 20 GeV/c, more slowly. This change in slope is qualitatively consistent with an interpretation in terms of a

diffractive component of the cross section, varying slowly with energy and becoming dominant at higher energies. For $n \geq 4$, all the cross sections display an initial rapid rise from threshold; for $n<16$ this is seen to be followed by a flattening off of the cross section. For the lower multiplicities, $n=4$ and $n=6$, the cross section is seen to be decreasing slowly at high momenta, while for higher multiplcities, $n \geq 16$, σ_n is still rising steeply at the highest momentum plotted. Meanwhile the total inelastic cross section remains almost constant. Similar behavior is seen in pp and π^+p interactions,[15,16] as well as in K^-p events (Section IV). The form of the curves implies scaling, which is discussed below in Section V.

D. The Multiplicity Distribution

Some moments of the multiplicity distribution are given in Table II, together with corresponding results found at 50,[11] 100,[12] and 205 GeV/c.[13]

Our measured value for the mean charged particle multiplicity in inelastic π^-p interactions at 147 GeV/c is $\langle n \rangle = 7.40 \pm 0.04$. We have fitted the values of $\langle n \rangle$ at the four beam momenta both to a power law and to a logarithmic law in $s/s_o (s_o = 1(\mathrm{GeV})^2)$, with the results, respectively:

$$\langle n \rangle = (2.02 \pm 0.01)(s/s_o)^{0.231 \pm 0.001} ,$$

$$\chi^2/\mathrm{NDF} = 0.08/2, \text{ Confidence Level} = 0.96;$$

$$\langle n \rangle = (-1.2 \pm 0.1) + (1.53 \pm 0.03)\ln(s/s_o),$$

$$\chi^2/\mathrm{NDF} = 1.0/2, \text{ Confidence Level} = 0.61.$$

Both expressions fit the data very well. The power law fit has the lower χ^2 value, but the data are also consistent with the logarithmic formula.

The value found at 147 GeV/c for $\langle n \rangle / D$ is 2.09±0.02, where $D = (\langle n^2 \rangle - \langle n \rangle^2)^{\frac{1}{2}}$. Comparison with the results at other momenta listed shows that this ratio is consistent with being constant over the π^- momentum range 50-205 GeV/c; this linear variation of D with $\langle n \rangle$ also holds down to much lower values,[14] at least down to $\langle n \rangle = 3$. It holds as well for π^--nucleus interactions at 100 and 175 GeV/c, for targets ranging from carbon to uranium.[17] A similar relation appears to be valid for other particles as well (Section IV, and References 11, 15, 16).

IV. K^-p INTERACTIONS

A. Scanning for K^-p Interactions

The counter telescope system was employed in the search for K^-p interactions. The K^- particles in the film were identified by a computer scan of the data tapes using a program called K TRACE.[18] The wire chamber information was read for each frame of the film and the Čerenkov tag checked for each beam track. For the K^- tracks, the upstream trajectory was projected downstream through the field of the bubble chamber magnet, to predict where a non-interacting K^- would pass through the downstream PWC's. The predicted trajectory was then compared to the actual hits in the downstream wire planes. If the mean squared deviation for any K^- beam particle exceeded 1.0 mm^2, then the computed information for each beam particle in the frame was listed. The listed frames were checked by an experienced scanner and a physicist to identify the K^- track in the film by comparing the calculated coordinates of each beam particle with the film images. When the K^- track was identified, the scanner recorded whether an interaction occurred within the visible volume of the

bubble chamber and, if so, the prong count. Unambiguous identification and separation of the K^- interactions from possible π^- interactions was achieved for 99 percent of the listed kaons. Consideration of the probabilities of the possible ways to produce the observed configurations allowed us to resolve the remaining events statistically. This procedure added an uncertainty of ±5 tracks to the incoming beam flux and ±2 events to the interaction sample. All interactions seen on K^- tracks in the film were recorded and used for the determination of the total cross section, but to ensure accurate prong counting a fiducial cut was made for the topological cross sections. The effective fiducial volume length in the chamber was 69.8 cm for the total cross section and 57.1 cm for the topological cross sections.

B. K^-p Total and Topological Cross Sections

Table III shows the results of our scan of events produced by the 9059±13 kaons entering the bubble chamber. The raw charged particle multiplicity data obtained are listed in the Column 2, with 87 additional events found in the enlarged volume used only for determination of the total cross section. The corrected numbers appearing in Column 3 and the cross section values in Column 4 were arrived at by considering the following corrections.

(i) Contamination of the K^- Sample

The pion contamination of the Čerenkov signal is estimated to be of the order of 1/4 percent. Somewhat more significant is the contamination produced by kaons decaying into pions which remain in the beam. Similar decay into muons was not a problem as these were detected and tagged by the muon counter downstream of the PWC's.

Since the transverse momentum of the decay product is nearly the same for both decay modes and the branching ratio is well known, we studied the decay muons to estimate the π contamination, finding that 1.0±0.3 percent of our tagged K's are actually π's by the time they reach the bubble chamber. The appropriate correction has been applied to the cross sections.

(ii) Scanning Efficiency

The efficiency of the computer scanning technique for finding events was checked by applying this method of locating interactions to every beam track (not only K^-) for a small sample of film. A double visual scan, with an efficiency of 99 percent for n=2 and greater than 99.5 percent for n>2, yielded 516 observed events. Of these the program detected 512, two 2-prong and two 4-prong events having been missed. Accordingly, 1 percent of the total observed events was added to the data, equally divided between the two- and four-prong channels. The visual scanning efficiency was then applied to the resulting data.

(iii) Low t Losses and Other Corrections

The very small sample of two prong events in the K^-p data did not allow reliable estimation of the low momentum transfer loss by fitting the $d\sigma/dt$ distribution and extrapolating to t = 0. However, since the data were consistent with the π^-p data, we assumed the same corrections as for π^-p, which were described above (Section IIE(ii)). The division between the elastic and inelastic events was made by assuming the same ratio as determined for π^-p interactions in this experiment.

Other corrections were made as described in Section IIE(iii) - (v) for $\pi^- p$ interactions. All the effects were very small: the single odd-prong event, with n=3, was added to the n=4 group, on the assumption that it involved a missed short stub; six events were estimated to have unresolved V^o or γ vertices, and 6 of 11 expected Dalitz pairs were not identified.

After all the above corrections have been applied we find a $K^- p$ total cross section of 21.5 mb±1.0 mb, in agreement with the 20.57±0.09 mb reported by Carroll et al.[7] The $K^- p$ topological cross sections σ_n are plotted in Figure 5, as functions of the K^- momentum.[11,19,20,21] In the momentum region covered by Figure 5, the 2-prong cross section is declining with increasing p, the 4-prong cross section reaches a broad maximum, then decreases, the 6-prong and 8-prong cross sections level off, while the higher multiplicities continue to rise.

The parameters of the inelastic charged multiplicity distribution are listed in Table IV. There are no significant differences from the $\pi^- p$ parameters, at our level of statistical accuracy. The similarity between the $\pi^- p$ and $K^- p$ charged multiplicity distributions is shown also in Figure 3, where the topological cross sections σ_n for both interactions are plotted as a function of n.

The dependence of <n> on s for $K^- p$ interactions is shown in Fig. 6. The data have been fitted with both a power law and a logarithmic law in s/s_o, $s_o = 1(\mathrm{GeV})^2$, with the following results:

$$\langle n\rangle = (1.37\pm0.06)(s/s_o)^{0.31\pm0.01},$$

$$\chi^2/\mathrm{NDF} = 16.6/4, \text{ Confidence Level} = 0.002;$$

$$\langle n\rangle = (-0.78\pm0.23) + (1.39\pm0.07)\ln(s/s_o),$$

$$\chi^2/\mathrm{NDF} = 17.0/4, \text{ Confidence Level} = 0.002 .$$

As is clear from Figure 6, the low momentum data are much more heavily weighted than the point at 147 GeV/c. The fit has been extended over a much larger momentum interval than was used for the $\pi^- p$ data, and it appears that the parameters of the power law and logarithmic law are not constant over the whole range. Although there are no K^- data between 33.8 GeV/c and our point at 147 GeV/c, it is interesting to note that for K^+p interactions at 100 GeV/c, $\langle n \rangle = 6.65 \pm 0.31$,[22] which falls between the fitted lines and agrees with both within the error.

V. SCALING

Assuming Feynman scaling at asymptotic values of s, Koba, Nielson and Oleson (KNO)[23] have shown that as $s \to \infty$, $\langle n \rangle \sigma_n / \sigma_{inel}$ becomes a function of $n/\langle n \rangle$ only:

$$\lim_{s \to \infty} (\langle n \rangle \sigma_n / \sigma_{inel}) = \psi(n/\langle n \rangle) \ . \qquad (2)$$

This prediction appears to be well satisfied even at rather low momenta, as shown by the $\pi^- p$ data in the momentum interval from 50 to 205 GeV/c, plotted in Fig. 7. No other $K^- p$ data are available in this momentum region, but a KNO plot for $K^- p$ is given in Fig. 8, to compare the data of this experiment at 147 GeV/c with the low momentum data, 4.2 GeV/c - 33.8 GeV/c.[21] Even over this wide range of momenta, scaling seems to hold within the experimental errors. In addition, the $\pi^- p$ and $K^- p$ plots are similar to each other, and, as shown in Fig. 9, follow closely Slattery's empirical fit to corresponding data for pp collisions between 50 and 303 GeV/c.[24]

A related scaling function[12,25] which emphasizes lower multiplicities is

$$\lim_{s \to \infty} (n \sigma_n / \sigma_{inel}) = \phi(\langle n \rangle / n) \ . \qquad (3)$$

Fig. 10 shows $n\sigma_n/\sigma_{inel}$ plotted vs $\langle n \rangle / n$ for our $\pi^- p$ and $K^- p$ data at 147 GeV/c. These points lie very close to a line drawn to represent other $\pi^- p$, pp and

π^+p data. (See Reference 12, and papers cited therein.)

VI. CONCLUSION

Total, elastic, and topological cross sections have been determined for π^-p and K^-p interactions at a beam momentum of 147 GeV/c, using the hybrid PWC-Bubble Chamber System. Moments of the multiplicity distributions have been obtained. Comparison with other data show that KNO scaling holds, starting at momenta at least as low as 50 GeV/c, and that very similar behavior in σ_n is shown over the momentum region 50 - 300 GeV/c, for π^-, π^+, K^- and protons.

Acknowledgements

We are please to acknowledge the excellent assistance of the FNAL Neutrino Section and the 30-inch bubble chamber staff in carrying out this experiment. We also thank the personnel of the participating universities, and the staff of the MIT PEPR for their skillful and efficient work.

FOOTNOTES

1. D. Fong et al., Phys. Letters 53B, 290 (1974).

2. J. Lach and S. Pruss, "Instrumentation of the Hadron Beams in the Neutrino Area", Fermilab Report TM-298 (1971).

3. W. Bugg, PHS Consortium Notes 28 and 30, 1974; W. Bugg et al., BAPS 18, 564 (1973) - program SURVEY.

4. T. Watts et al. BAPS 18, 564 (1973) - program PWGP.

5. E. S. Hafen, APC Programming Note, DAS 75-1, 1975; F Bruyant et al., BAPS 19, 96 (1974).

6. D. Fong, PHS Consortium Note 33, 1974.

7. A. S. Carroll et al., Phys. Rev. Letters 33, 932 (1974).

8. E. B. Brucker et al., BAPS II 20, 546 (1975).

9. V. Chaloupka et al., Phys. Letters 50B, 2 (1974).

10. D. Fong et al., Inelastic Two-Prong Events in 147 GeV/c $\pi^- p$ Collisions, July 1975, submitted to Nuclear Physics B.

11. G. A. Akopdjanov et al., Nucl. Phys. B75, 401 (1974).

12. E. L. Berger et al., Nucl. Phys. B77, 365 (1974).

13. D. Bogert et al., Phys. Rev. Letters 31, 1271 (1973).

14. A. Wroblewski, Acta Phys. Pol. B4, 854 (1973). (A Compilation of low energy data.)

15. J. Whitmore, Physics Reports 10, 273 (1974). A review article; see also references cited therein.

16. H. Bøggild and T. Ferbel, Annual Rev. of Nucl. Science 24, 451 (1974). A review article; see also reference cited therein.

17. W. Busza et al., Phys. Rev. Letters 34, 836 (1975).

18. K TRACE, developed from SURVEY (Ref. 3) by W. Bugg and D. Petersen.

19. V. V. Ammosov et al., Nuclear Physics B58, 77 (1973), and references cited therein.

20. J. R. Fry et al., Nuclear Physics B58, 408 (1973).

21. D. Kuhn, CERN/D. PH II/ Phys. 74-37 and Fortshritte der Physik (in press); and references cited therein.

22. V. E. Barnes et al., Phys. Rev. Letters 34, 415 (1975).

23. Z. Koba et al., Nucl. Phys. B40, 317 (1972).

24. P. Slattery, Phys. Rev. Letters 29, 1624 (1972).

25. M. J. Counihan, Nuovo Cimento Letters 9, 561 (1974).

TABLE I

TOPOLOGICAL CROSS SECTIONS IN 147 GeV/c $\pi^- p$ INTERACTIONS

Number of charged prongs, n	Number of events seen		Corrected number of events, N_n	Cross Section[b] (mb)
2	2888		3248.0±93.4[a]	5.04±0.15
		Elastic	2087.3±85.1	3.24±0.14
		Inelastic	1160.7±69.3	1.80±0.12
3	22			
4	2442		2657.3±62.5	4.12±0.10
5	7			
6	2752		2881.1±61.1	4.47±0.10
7	12			
8	2593		2769.7±64.6	4.30±0.11
9	32			
10	1890		1991.7±55.8	3.09±0.09
11	21			
12	1097		1145.5±42.8	1.78±0.07
13	27			
14	534		533.5±30.3	0.83±0.05
15	22			
16	253		250.7±19.8	0.39±0.03
17	11			
18	98		95.0±12.0	0.15±0.02
19	2			
20	37		34.9±6.5	0.054±0.010
21	1			
22	5		4.5±2.3	0.0070±0.0036
23				
24	3		3.1±1.8	0.0048±0.0028
25				
26	1		1.0±1.0	0.0016±0.0016
TOTAL	14750			24.24±0.29

a) The number of two-prong events in Column 2 was found in a somewhat longer fiducial volume than was used for n>2. In column 3, this number has been normalized to the same scanning length.

b) These figures are the cross sections as determined from this experiment; they are not normalized to any other absolute measurement. The listed errors include statistical errors and the uncertainties in the corrections, as well as uncertainties in the determination of the total pion path length, the hydrogen density, and the elastic/inelastic assignment of 2-prong events.

TABLE II

MOMENTS OF THE MULTIPLICITY DISTRIBUTION FOR $\pi^- p$ INTERACTIONS AT VARIOUS MOMENTA

	50[c]	100[d]	147	205[e]
$\langle n \rangle$	5.78±0.04	6.79±0.08	7.40±0.04	8.02±0.12
$\langle n(n-1) \rangle$	34.9±0.48	49.±1.	59.9±0.7	71.6±1.8
$\langle n^2 \rangle$	40.7±0.48	56.±1.	67.3±0.7	79.6±1.8
f_2[a]	1.53±0.15	3.2±0.3	5.14±0.22	7.24±0.61
D[b]	2.70±0.03	3.16±0.04	3.54±0.03	3.91±0.11
$\langle n \rangle / D$	2.14±0.03	2.15±0.04	2.09±0.02	2.05±0.05

a) $f_2 = \langle n(n-1) \rangle - \langle n \rangle^2$

b) $D = (\langle n^2 \rangle - \langle n \rangle^2)^{\frac{1}{2}}$

c) Reference 11

d) Reference 12

e) Reference 13

TABLE III

TOPOLOGICAL CROSS SECTIONS IN 147 GeV/c K^-p INTERACTIONS

Number of charged prongs, n	Number of events seen		Corrected number of events, N_n	Cross Sectio (mb)
2	69		81±10	4.27±0.53
		elastic	52±8	2.74±0.42
		inelastic	29±6	1.53±0.32
3	1			
4	64		68±9	3.59±0.47
5	0			
6	90		90±11	4.75±0.58
7	0			
8	60		62±9	3.27±0.47
9	0			
10	62		62±9	3.27±0.47
11	0			
12	26		25±6	1.32±0.3[illegible]
13	0			
14	10		9±4	0.47±0.21
15	0			
16	3		3±2	0.16±0.11
17	0			
18	7		6±3	0.32±0.16
19	0			
20	2		2±1	0.11±0.05
TOTAL	394			
FULL VOLUME	481		496±22	21.5±1.0

TABLE IV

MOMENTS OF THE MULTIPLICITY DISTRIBUTIONS FOR K^-p INTERACTIONS AT 147 GeV/c

$\langle n \rangle$	7.33 ± 0.21
$\langle n(n-1) \rangle$	58.7 ± 3.7
$\langle n^2 \rangle$	66.0 ± 3.9
f_2 [a]	5.0 ± 1.1
D [b]	3.51 ± 0.17
$\langle n \rangle / D$	2.09 ± 0.09

a) $f_2 = \langle n(n-1) \rangle - \langle n \rangle^2$

b) $D = (\langle n^2 \rangle - \langle n \rangle^2)^{1/2}$

FIGURE CAPTIONS

Fig. 1 Schematic diagram of the Hybrid PWC-30-inch Bubble Chamber System, showing the locations of counters upstream and downstream of the bubble chamber. The muon detector, which is located downstream of the telescope, is not shown. The trajectories of the particles in a typical 2-prong event are sketched in.

Fig. 2 $d\sigma/dt$ vs $-t$, the momentum transfer to the proton, for elastic events. The line is a fit to the points over the interval $0.04 \leq |t| < 0.6$ $(GeV/c)^2$. It has the form $d\sigma/dt = 26.9 \exp(-8.29|t|)$.

Fig. 3 Topological cross sections σ_n vs n, for $\pi^- p$ and $K^- p$ interactions at 147 GeV/c.

Fig. 4 Topological cross sections σ_n vs beam momentum (laboratory) for $\pi^- p$. The data points at $p_{\pi^-} = 147$ GeV/c, indicated by an arrow, are from this experiment. Data at other momenta are from references 11-13, and references cited in 14 for $p_{\pi^-} < 50$ GeV/c. The lines are drawn through the data points to guide the eye.

Fig. 5 Topological cross sections σ_n vs beam momentum (laboratory) for $K^- p$. The data points at $p_{K^-} = 147$ GeV/c, indicated by an arrow, are from this experiment. Data at other momenta are from references 11, 19, 20, and 21. The lines are drawn through the data points to guide the eye.

Fig. 6 Charged particle multiplicity $\langle n \rangle$ vs s for $K^- p$ interactions. The solid and dashed lines are fits to the data of functions of the form $\langle n \rangle = a + b \ln(s/s_o)$ and $\langle n \rangle = a(s/s_o)^b$, respectively.

Fig. 7 KNO scaling function $\langle n\rangle\sigma_n/\sigma_{inel}$ vs $n/\langle n\rangle$, for π^-p interactions at 147 GeV/c, and for other π^-p data at 50, 100, 205 GeV/c, from References 11-13.

Fig. 8 KNO scaling function $\langle n\rangle\sigma_n/\sigma_{inel}$ vs $n/\langle n\rangle$, for K^-p interactions at 147 GeV/c, and for low-momentum K^-p data from Reference 21.

Fig. 9 The KNO scaling function $\langle n\rangle\sigma_n/\sigma_{inel}$ vs $n/\langle n\rangle$. Points are plotted for π^-p and K^-p at 147 GeV/c. The solid line is an empirical fit to the data for pp collisions from 50-300 GeV/c (Reference 24).

Fig. 10 The scaling function $n\sigma_n/\sigma_{inel}$ vs $\langle n\rangle/n$. The solid line is one drawn by eye through points (not shown) from π^-p, π^+p and pp interactions in the range 50-300 GeV/c. The points are the data of this experiment for π^-p and K^-p at 147 GeV/c.

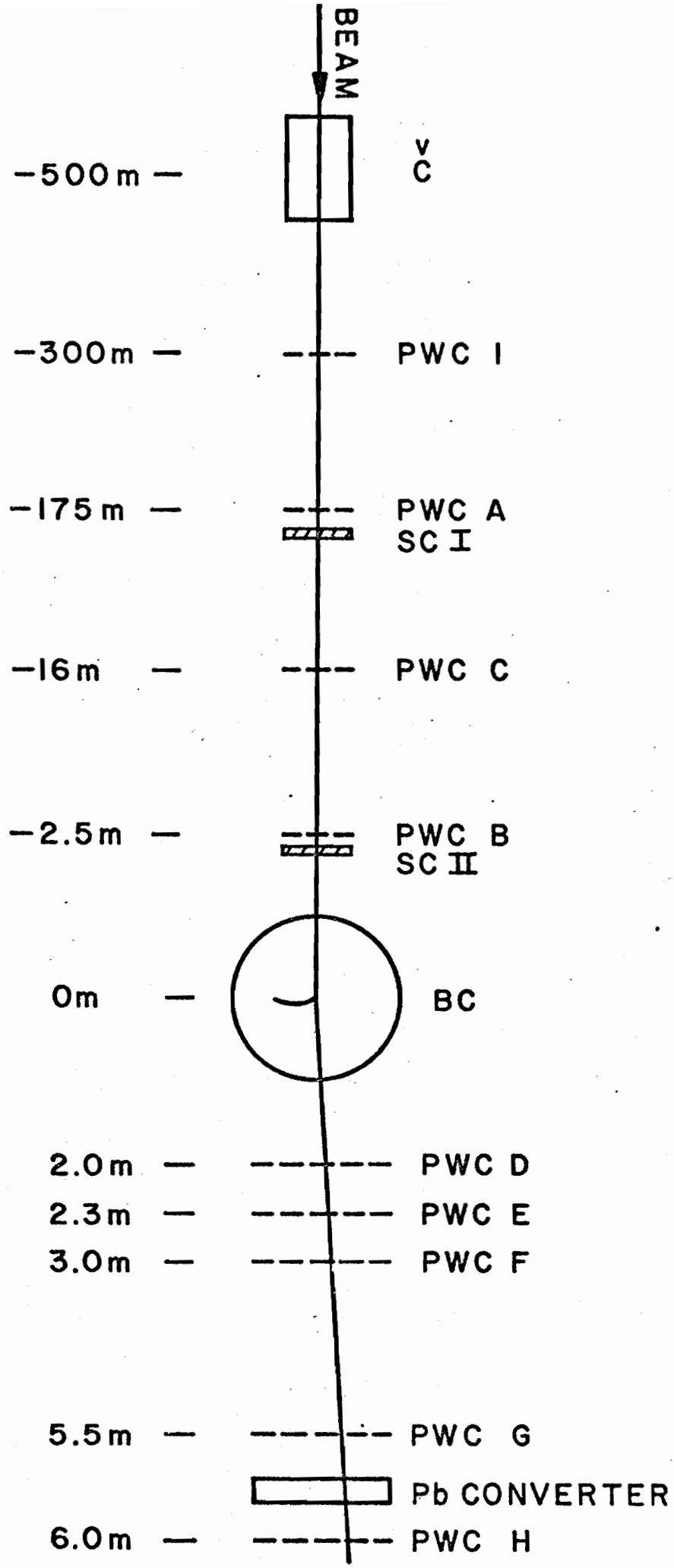
BEAM
-500 m
v
C
-300 m
PWC I
-175 m
PWC A
SC I
-16 m
PWC C
-2.5 m
PWC B
SC II
0 m
BC
2.0 m
PWC D
2.3 m
PWC E
3.0 m
PWC F
5.5 m
PWC G
Pb CONVERTER
6.0 m
PWC H

FIGURE

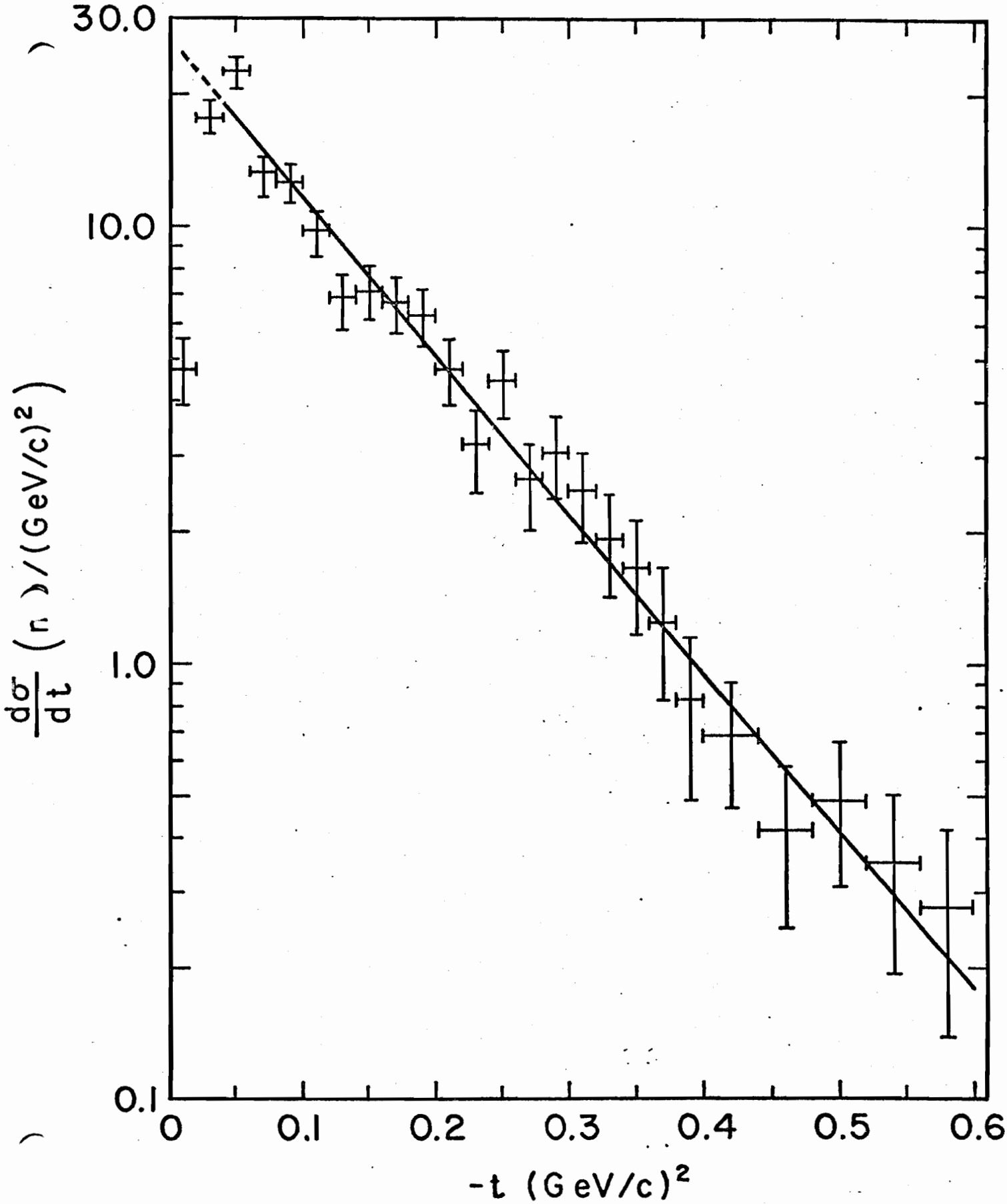

FIGURE 2

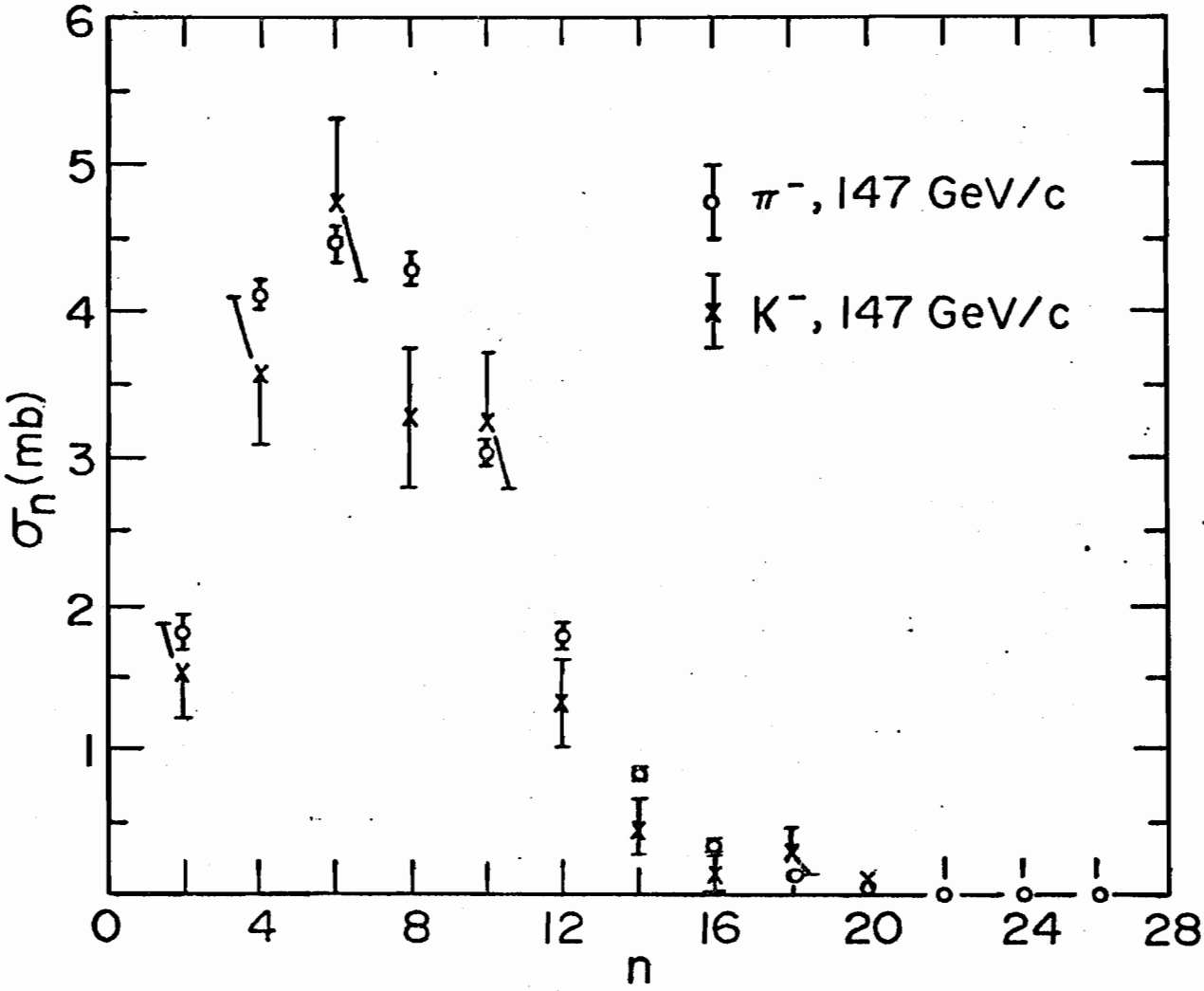

FIGURE 3

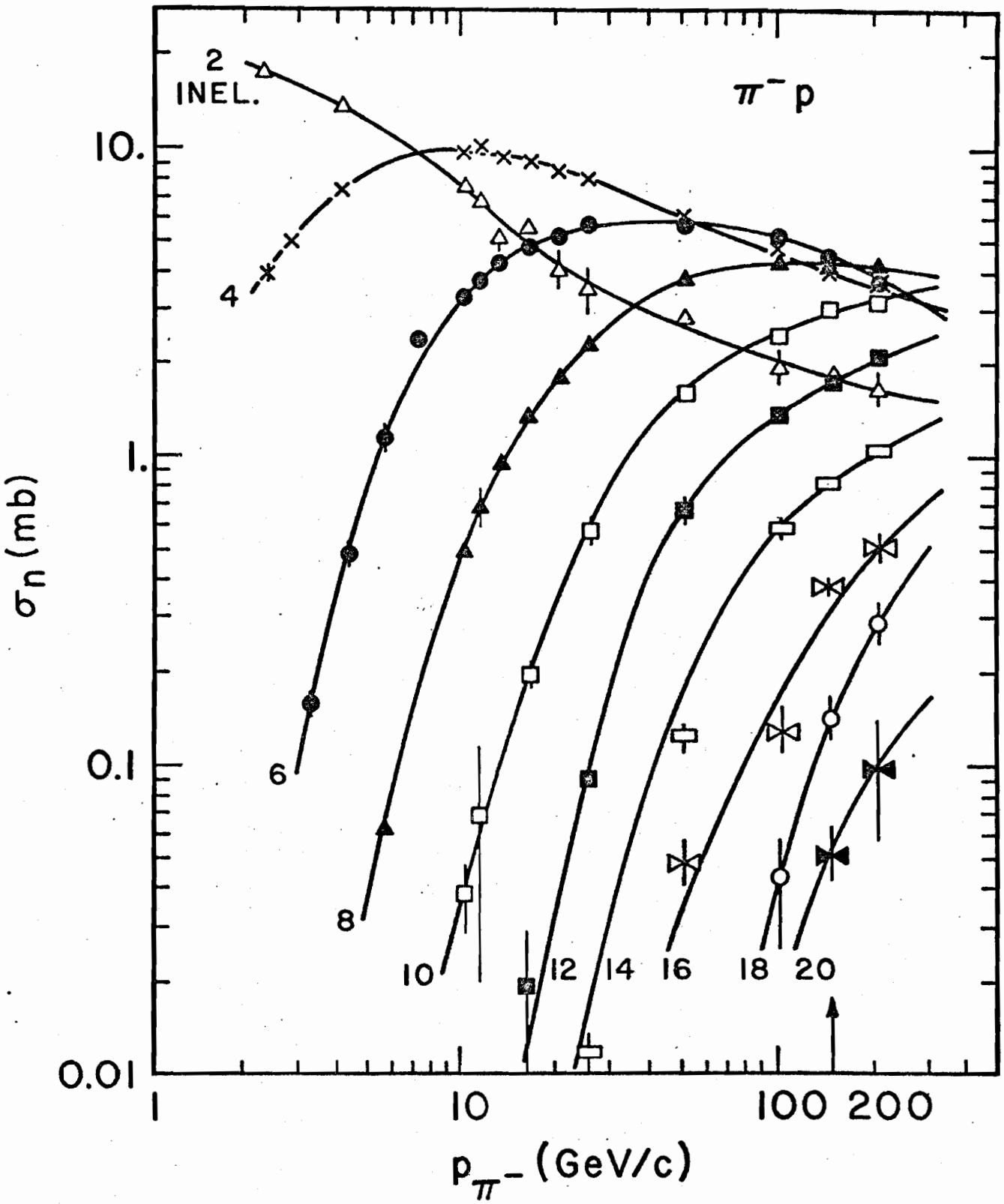
2
INEL.
$\pi^- p$
4
6
8
10
12
14
16
18
20
10.
1.
0.1
0.01
σ_n (mb)
1
10
100
200
p_{π^-} (GeV/c)

FIGURE 4

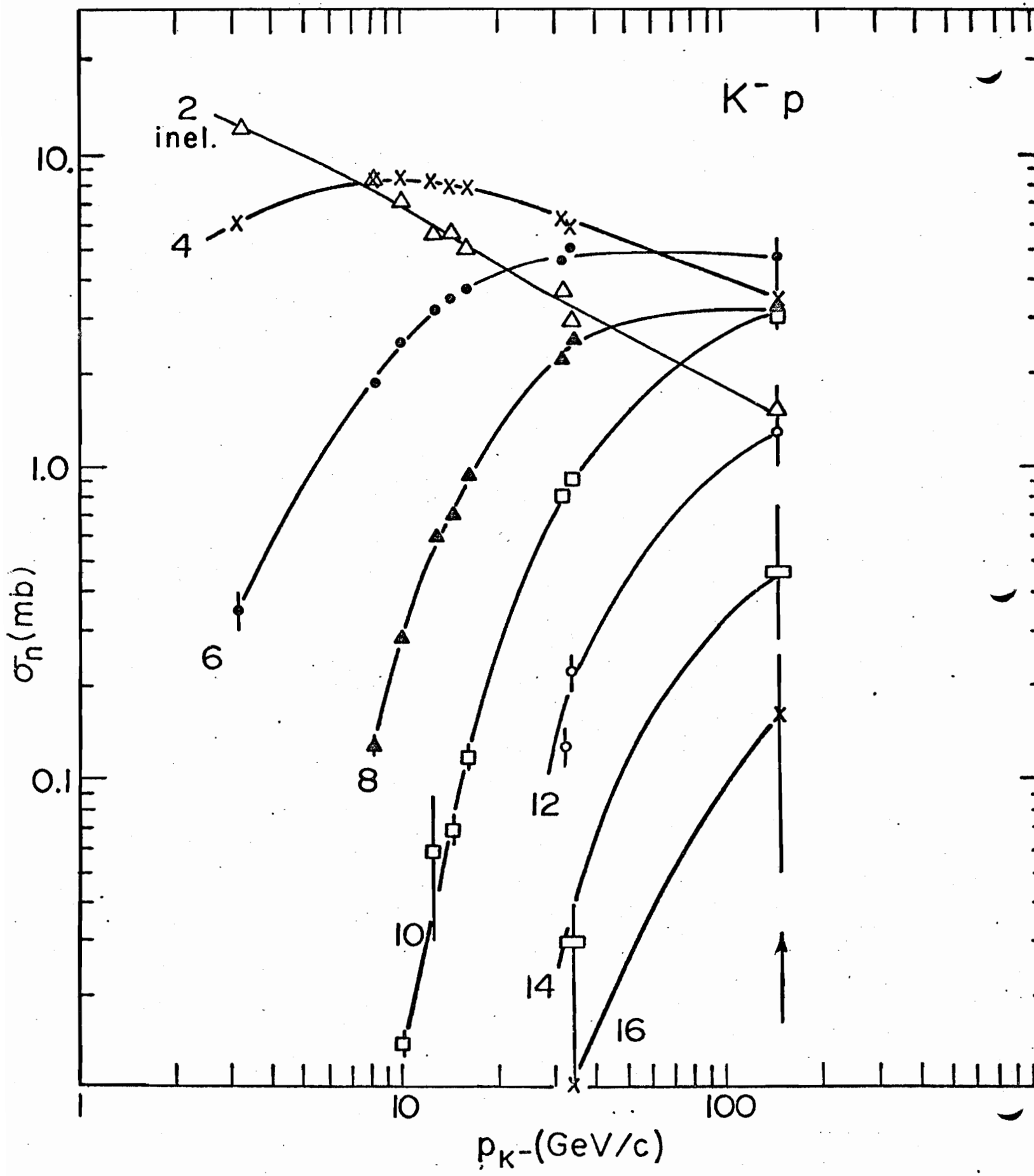

FIGURE 5

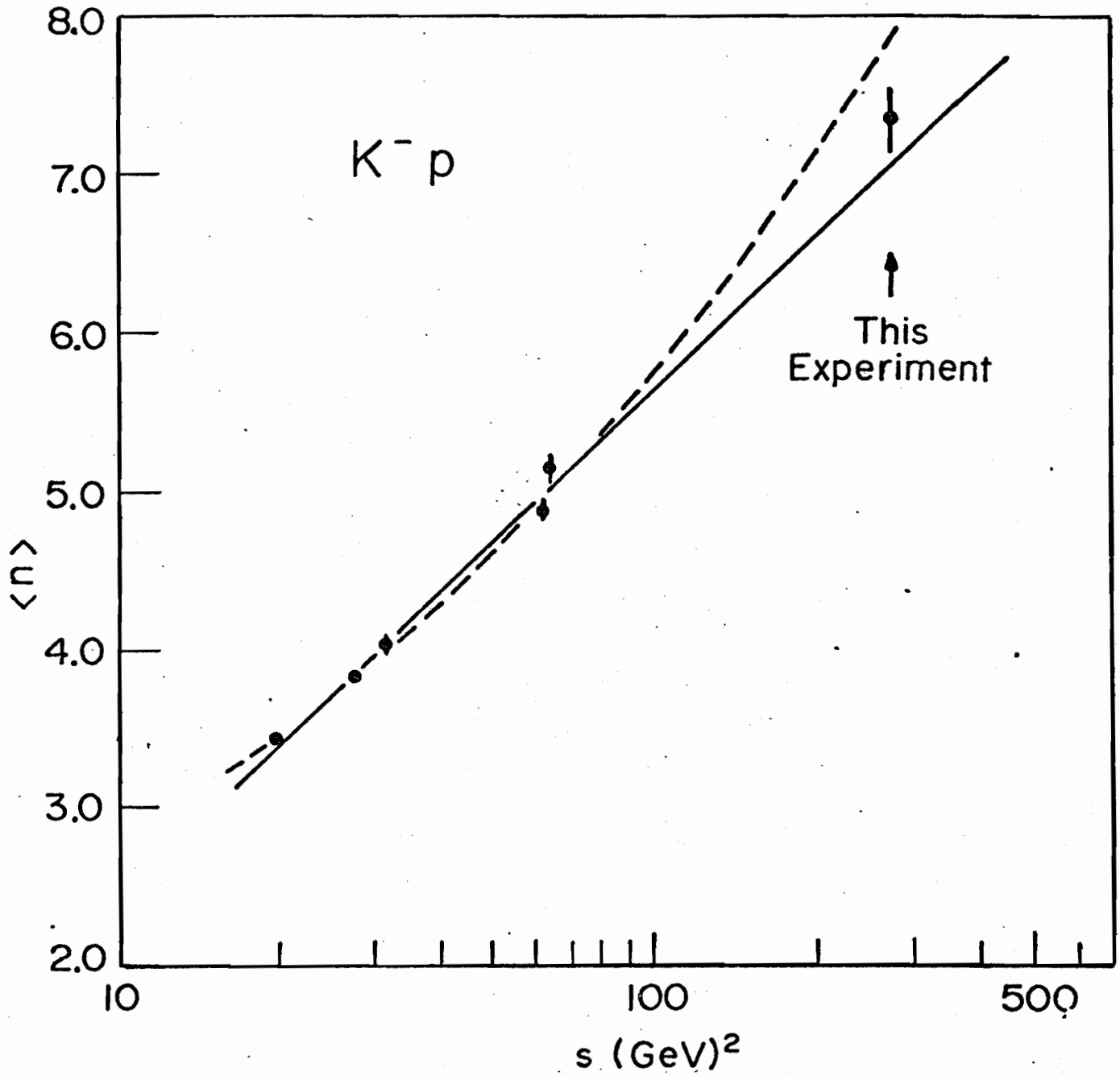

FIGURE 6

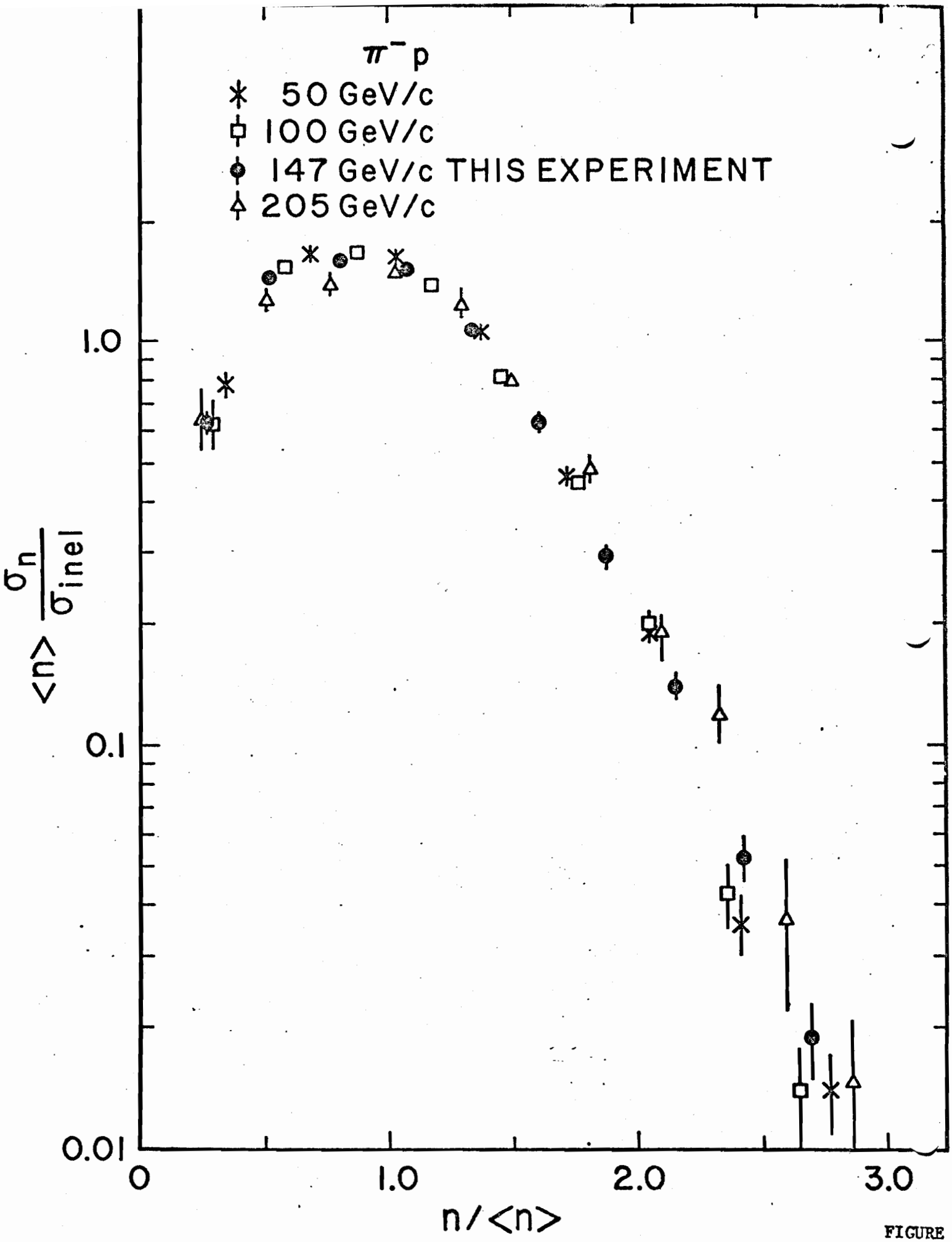
$\pi^- p$
50 GeV/c
100 GeV/c
147 GeV/c THIS EXPERIMENT
205 GeV/c
1.0
0.1
0.01
$\frac{\sigma_n}{\sigma_{inel}} \langle n \rangle$
0
1.0
2.0
3.0
$n/\langle n \rangle$

FIGURE

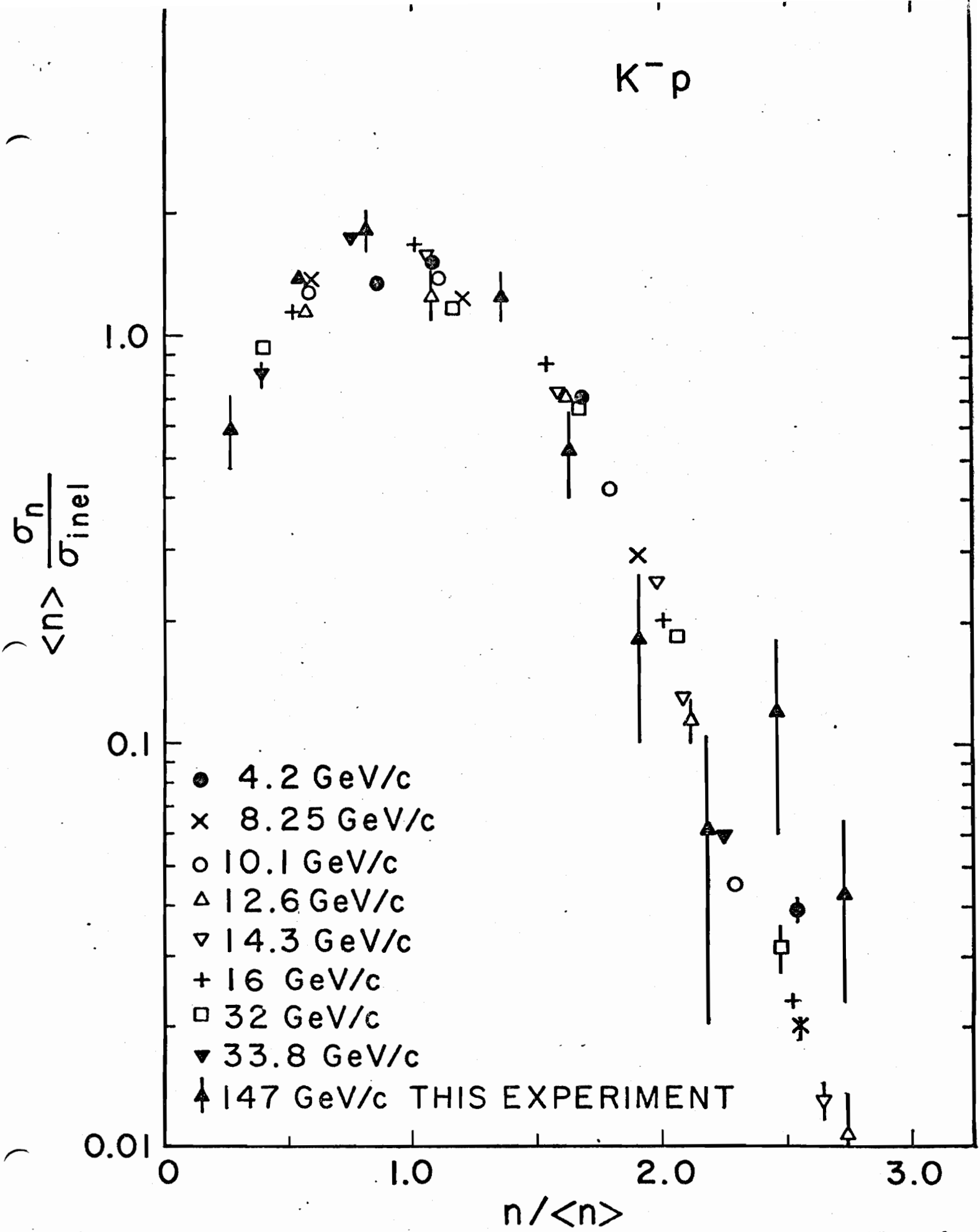
K⁻p
1.0
0.1
0.01
0
1.0
2.0
3.0
n/<n>
<n> σn/σinel
4.2 GeV/c
8.25 GeV/c
10.1 GeV/c
12.6 GeV/c
14.3 GeV/c
16 GeV/c
32 GeV/c
33.8 GeV/c
147 GeV/c THIS EXPERIMENT

FIGURE 8

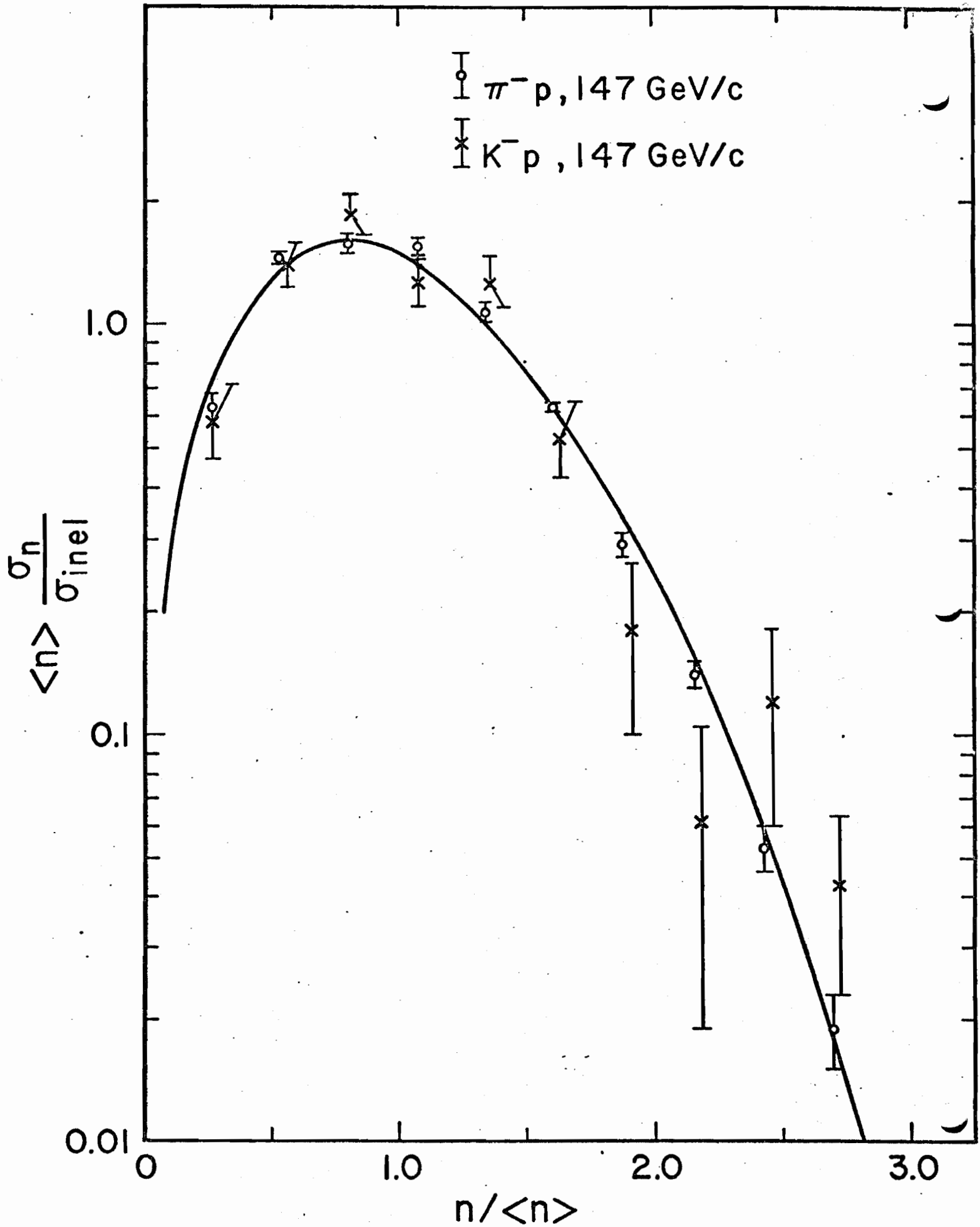

FIGURE 9

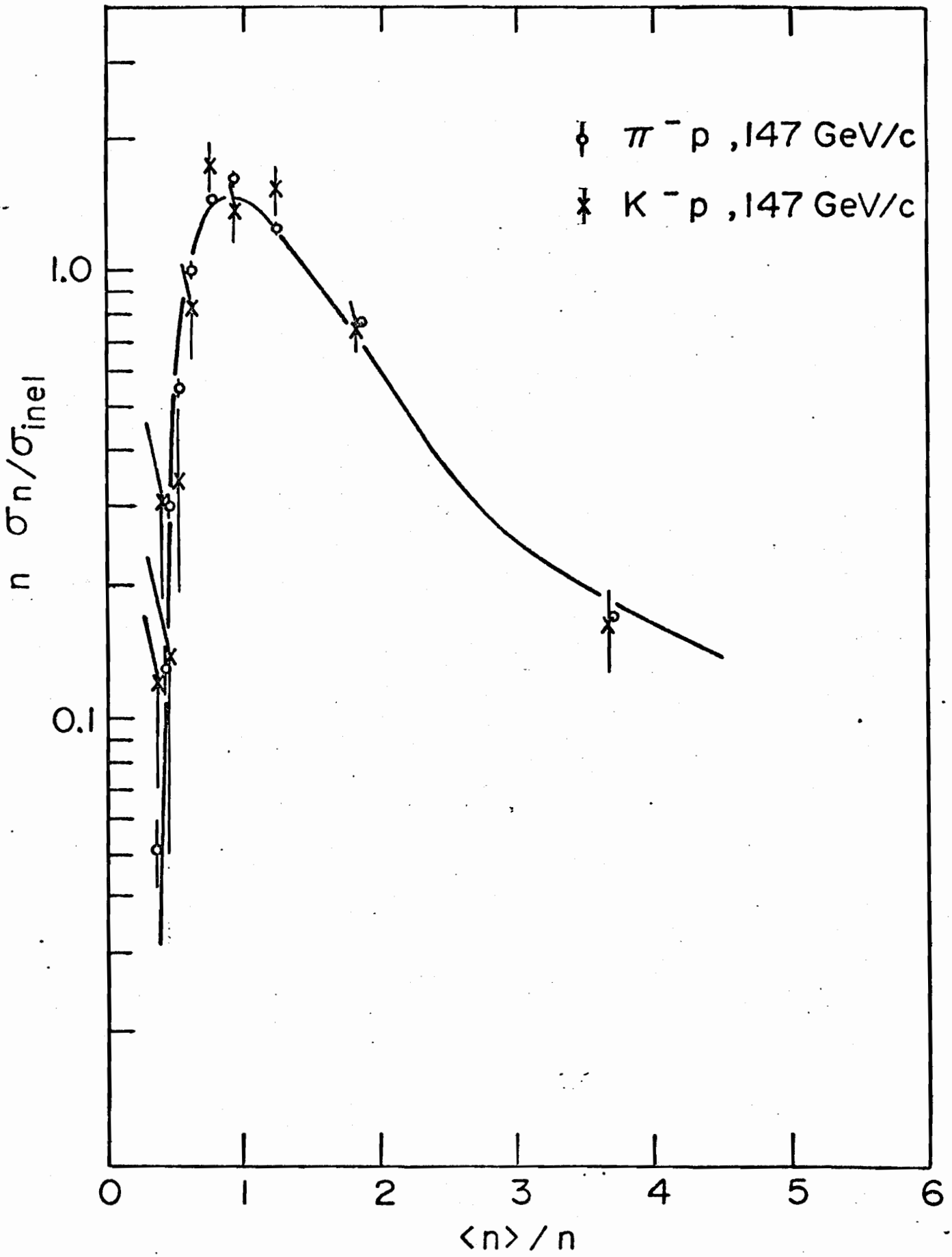

FIGURE 1(